Atomic Spectroscopy

Article

Elemental Quantitative Imaging Analysis of $Bi_4Si_3O_{12}$ Crystals Defects by LA-ICP-MS

Yuquan Xu,[a,b] Zhaoqing Cai,[b,c] Wenxin Cui,[b] Qing Li,[b] Jiayue Xu,[a,*] and Zheng Wang [b,c,*]

[a] School of Materials Science and Engineering, Shanghai Institute of Technology, Shanghai 201418, P. R. China

[b] Shanghai Institute of Ceramics, Chinese Academy of Sciences, Shanghai 201899, P. R. China

[c] Center of Materials Science and Optoelectronics Engineering, University of Chinese Academy of Sciences, Beijing 100049, P. R. China

Received: *March 21, 2022;* ***Revised:*** *April 30, 2023;* ***Accepted:*** *May 02, 2023;* ***Available online:*** *May 02, 2023.*

DOI: 10.46770/AS.2023.080

ABSTRACT: In this study, a laser ablation inductively coupled plasma mass spectrometry (LA-ICP-MS) method is developed for in -situ quantitative imaging of trace impurity elements in $Bi_4Si_3O_{12}$ (BSO) crystals. This method has unique advantages of low detection limit and high spatial resolution for the analysis of defects in crystal microregions. The regression coefficients of the calibration curves for each element were greater than 0.99, and the detection limits (DLs) were 17, 5, 7, 48, 5, 7, 16, 27, and 7 ng/g for ^{24}Mg, ^{45}Sc, ^{48}Ti, ^{90}Zr, ^{139}La, ^{146}Nd, ^{172}Yb and ^{208}Pb, respectively. The LA-ICP-MS measurements were in good agreement with the results obtained using conventional ICP-MS method. Segregation phenomena of elemental impurities in the axial direction of the BSO crystal can exist during crystal growth. Finally, the distribution of the impurity elements in the dendritic crystal defect region of the crystal was visualized. We believe that this work proposes a novel less-invasive analysis method for exploring the composition-defect relationship of crystals.

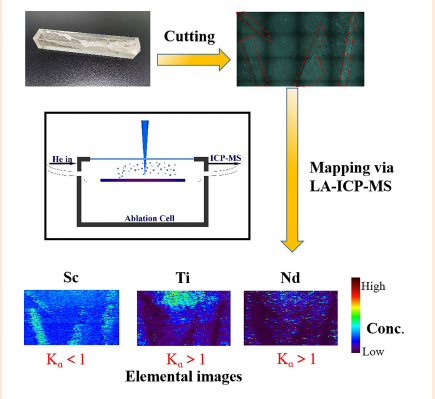

INTRODUCTION

Scintillation crystals are functional crystal that can produce visible light under the impact of high-energy rays (particles) that can be recorded by photoelectric counters. They are widely used in high-energy physics, nuclear physics, nuclear medicine imaging, safety inspection, and geological exploration among other fields.[1-3] $Bi_4Si_3O_{12}$ (BSO) crystals are scintillation material of wide interest because of its good mechanical properties, stable chemical properties and good optoelectronic properties.[4,5] Additionally BSO crystals are significantly cheaper than other scintillation crystals, which is advantageous for the construction of large high-energy leptonic colliders.[6-9] The shorter UV absorption edge of BSO crystals separates Cherenkov light and scintillation light effectively, and thus, the crystals can collect Cherenkov light signals efficiently. Therefore, BSO crystals are among the best candidates for homogeneous hadron calorimeters and double readout calorimeters.[10]

When single crystals are grown using the Bridgman method, the impurities seriously affect the properties and growth integrity of BSO crystals.[11-13] Despite better crystal growth from purer the materials, it is practically impossible to use pure raw materials because of their high cost.[14, 15] However, not all impurities are harmful. Therefore, after clarifying the relationship between impurities and crystal defect formation, it is important to strictly limit the harmful impurities and consciously add the beneficial ones. However, the distribution of impurity elements in BSO crystals, particularly the crystal defects, remains unclear.

Conventional elemental analysis are mainly performed using atomic spectrometry[16, 17] and inductively coupled plasma mass spectrometry (ICP-MS).[18, 19] However, all these techniques require the crystal sample to be digested, and, thus, they only provide information on the average content of elements in the whole crystal, while ignoring information on the spatial distribution. To date, X-ray fluorescence spectroscopy (XRF),[20-22] glow discharge

mass spectrometry (GD-MS),[23,24] secondary ion mass spectrometry (SIMS)[25,26] and electron probe microanalysis (EPMA)[27] have been the most suitable methods for in situ and elemental distribution analysis of solid materials. However, these methods have both advantages and disadvantages when applied to solid-sate analysis. Despite their high spatial resolutions, the detection limits (DLs) of EPMA and XRF are insufficient for the quantification of trace elements in crystals. Conversely, GD-MS and SIMS possess have low DLs, however, GD-MS analysis of non-conductive samples requires complex processing steps, and SIMS can only analyze known elements. Therefore, to analyze the relationship between the impurity elements and defect formation in crystals, a method should be developed that can directly and sensitively detect trace impurities and analyze the distribution of impurity elements in the microregions of defects.

Laser ablation inductively coupled plasma mass spectrometry (LA-ICP-MS) is an analytical method for solid samples that has advantageous properties such as wide dynamic range, multi-element detection, high sensitivity (μg/g to ng/g), and high spatial resolution (~μm).[28-31] Therefore, LA-ICP-MS is applied for the elemental analysis in crystal samples, such as the imaging of lanthanum in an alumina ceramic tube,[32] and analysis of doping elements in BaF_2 crystals,[33] and diffusion behavior of Cr in ZnS crystals.[34] However, to the best of our knowledge, LA-ICP-MS has been used in only a for few studies based on impurity distribution in BSO crystals, and has not been used, to explore the relationship between impurity distribution and defect formation.

In this study, the effect of the distribution of trace impurities in the crystal on the formation of crystal defects was investigated by LA-ICP-MS. To provide useful information on the growth of high-quality crystals, matrix matched calibration standards were prepared, ^{29}Si was selected as the internal standard (IS) element, and LA-ICP-MS was used to quantitatively analyze impurity elements in BSO crystals and quantitatively image dendritic crystal defects in the crystals to establish the relationship between impurity elements and crystal defect formation.

EXPERIMENTAL

Instruments. A laser ablation system (NWR-213, ESI, USA) and quadruple ICP-MS system (ICAP RQ, Thermo Fisher, USA) were combined to perform LA-ICP-MS analysis. ^{24}Mg, ^{45}Sc, ^{48}Ti, ^{90}Zr, ^{139}La, ^{146}Nd, ^{172}Yb, and ^{208}Pb with significant signals in pre-experiments were selected. The operational parameters and isotopes are listed in Table 1. PN-ICP-MS (X Seriers 2, Thermo Fisher Scientific, USA) was used for the quantitative analysis of the digested samples. A pellet presser (769YP-30T, Keqi, China) was used to press $Bi_4Si_3O_{12}$ powder into pellets. The samples were pulverized using a ball mill (RS 200, Retsch, Germany). The

Table 1. Operation parameters for LA-ICP-MS experiments

LA parameters	Value	ICP-MS parameters	Value
Laser ablation system	NWR-213	ICP-MS instrument	ICAP RQ
Laser wavelength (nm)	213	RF power (W)	1350
Laser frequency (Hz)	20	Cooling gas (Ar) (L/min)	800
Laser energy (J/cm^2)	8.25	Make-up gas (Ar) (L/min)	1200
Ablation spot size (μm)	60	Detector mode	Dual
Scan rate (μm/s)	35	Isotopes	^{24}Mg, ^{29}Si, ^{45}Sc, ^{48}Ti, ^{90}Zr, ^{139}La, ^{146}Nd, ^{172}Yb, ^{208}Pb

samples were weighed using a precision electronic balance (AE 240, METTLER, Switzerland). During LA-ICP-MS analysis, the sample was ablated under a constant stream of helium, which was mixed with argon as a makeup gas before introduction into the ICP-MS instrument.

Reagent and sample. High purity Bi_2O_3 and SiO_2 (99.999 wt %, Shanghai Reagent Factory, China) were used to prepare matrix-matched calibration standards. High quality 68 wt % HNO_3 and 40 wt % HF (GR, Shanghai Aoban Technology Co., Ltd., China) were used for samples digestion. The solutions were prepared in deionized water (DIW). Multi-element standards were prepared from 1000 mg/L water-based standards (Inorganic Ventures, USA). The two BSO crystal samples used were provided by the Shanghai Institute of Ceramics, Chinese Academy of Sciences. One sample was defect-free and homogeneous for the quantitative analysis, while the other sample had a large number of dendritic crystal defects and was used for imaging analysis. DIW (R = 18.25 MΩ·cm) obtained from a Milli-Q water system (Millipore, Bedford, USA) was used for the preparation of all solution blanks standards.

Preparation of matrix-matched calibration standards. To prepare matrix-matched calibration standards calibration standards polycrystalline BSO powders were prepared using a two-step sintering method. SiO_2 and Bi_2O_3 powders were dried at 300 °C for 3 h and then weighed according to their respective stoichiometries. The weighed powder was mixed in a ball mill coated with polyethylene for 8 h, and maintained at 800 °C for 8 h. After sintering, it was ground into a powder and mixed again in a ball mill for 3 h. The samples were then placed in an aluminum oxide crucible and held at 850 °C for 12 h to obtain pure polycrystalline BSO powder.

BSO polycrystalline powder (4.0 g) was mixed with different volumes (0, 10, 20 and 40 μL) of 1000 mg/L multi-element aqueous standard solution and 20 mL of water. The suspension was stirred for 10 min, left to stand overnight, heated at 100 °C for 5 h, and then dried to afford a homogeneously mixed powder. Dried mixture (~1.0 g) was pressed into a pellet with a diameter of 1 cm at 15 MPa for 2.5 min. The pellets from both procedures were stored separately in clean plastic bags prior to LA-ICP-MS analysis.

Method validation. As there are no specific certified values for the various trace elements in the crystals, the reference value for each element was determined by ICP-MS analysis. To this end, 0.1 g of BSO crystal was added to a PTFE vessel and heated with 10 mL HF and 5 mL HNO_3 at 160 °C until the sample was completely dissolved. The solution was cooled and diluted to 40 mL with DIW. The digested solution was analyzed using ICP-MS to verify the accuracy of the LA-ICP-MS quantification results.

Imaging. NWR image laser ablation system (ESI, USA) with a 213-nm Nd:YAG laser and a high performance two-volume ablation chamber(TwoVo I) was used for imaging. A quadrupole ICP-MS system (ICAP RQ, Thermo Fisher Scientific, USA) was coupled with the NWR image laser ablation system for quantitative elemental imaging. Prior to imaging, the instrument was optimized by ablating the standard reference material NIST SRM 612 to obtain maximum signals of $^{115}In^{+}$ and $^{238}U^{+}$ and minimum ratios of $^{140}Ce^{16}O/^{140}Ce^{+}$ and $^{140}Ce^{2+}/^{140}Ce^{+}$.

The isotopes ^{24}Mg, ^{29}Si, ^{45}Sc, ^{48}Ti, ^{90}Zr, ^{139}La, ^{146}Nd, ^{172}Yb and ^{208}Pb were evaluated throughout the experiments, and the signal of ^{29}Si was used as the IS to calibrate instrument signal drift. For crystal samples imaging, the spot size was 35 μm as a compromise between spatial resolution and ablation time. The laser frequency was 10 Hz, scan speed was 35 μm/s, and carrying gas flow rate was set to 750 mL/min to optimize the washout time as much as possible. Origin 2020 was used for data manipulation, and image integration was performed using Iolite v4.0 software, which is based on Igor7.

Fig. 1 Powder XRD pattern of the $Bi_4Si_3O_{12}$ synthesized using SiO_2 and Bi_2O_3. The calculated powder XRD pattern is shown in black for comparison.

RESULTS AND DISCUSSION

Phase analysis and homogeneity characterization of calibration standards. To verify that the prepared solid standard was consistent with the crystalline phase of the crystals, the samples were ground, and their XRD patterns were obtained (Fig. 1). According to PDF#33-0215, the XRD pattern of the sintered sample contained diffraction peaks and relative intensities very similar to those of $Bi_4Si_3O_{12}$, with no significant peak shifts or secondary phases. This indicated that a pure BSO phase polycrystalline powder that matched the matrix was obtained.

The homogeneity of the matrix-matched calibrant is an important criterion for assessing the reliability of the calibration standards. To verify homogeneity, LA-ICP-MS was applied in multi-line scanning mode. Fig. 2 shows the signal intensities of the trace analyte elements in the BSO standard, obtained by LA-ICP-MS ablation. The results shown in Fig. 2 indicate a uniform distribution of trace elements in the matrix-matched BSO standards, and these results are reproducible. The relative standard deviations were less than 10% for all elements without IS correction. These results illustrate that a homogenous distribution of trace elements was achieved using the facile approach developed in this study.

Fig. 2 Time-resolved signals of analytes in a matrix-matched calibrant analyzed directly by LA-ICP-MS

Quantification of trace impurity elements in crystals. Si was the main component in the BSO crystal samples and was uniformly distributed throughout the samples. The lower abundance isotopes (^{28}Si, ^{29}Si, and ^{30}Si) could be used as IS because of the high silicon content in BSO. Therefore, ^{29}Si was selected as the IS to quantify trace impurity elements in the BSO crystals using the widely used external calibration and internal standardization calibration procedure. This calibration procedure involved measuring the intensity of a single isotope of each element and determining the relative sensitivity factor (RSF). The RSF is defined as follows:

Concentration (IS) × intensity (i) / concentration (i) × intensity (IS)

The RSF can be used to calculate the concentration of analytes as follows:

$$Concentration\ (i)_{sample} = Concentration\ (IS)_{sample} \times Intensity\ (i)_{sample} / Intensity\ (IS)_{standard} \times RSF_{standard}$$

where i represents the element of interest and IS represents the internal standard. In this study, the RSF obtained from the standard was used to calculate the analyte concentrations in the BSO crystal samples. Each standard was ablated three times with LA-ICP-MS. The average signal intensity values of three ablations were used to construct the calibration curve.

The linearity coefficients (R^2) of the calibration curve equations, limits of detection (LODs), quantitative results of ICP-MS, and results obtained from the LA-ICP-MS analysis are shown in Table 2. Certified values for the various trace elements were not available for determining the content of these elements in the BSO crystals. The measurement errors between the results of LA-ICP-MS and PN-ICP-MS analyse were less than 10 % (Table 2). The LODs were calculated as follows:

$$LOD=3SD/k$$

where SD is the standard deviation of the matrix blank signal obtained during laser preheating, and k is the slops of each calibration curve. The linear coefficients (R^2) of the calibration curve equations for all the elements were measured greater than 0.99. These indicate that the developed quantitative method is suitable and accurate for the quantitative analysis of trace elements in BSO crystals.

Distribution characteristics of impurity elements in crystals. The entry of impurities into the crystal lattice during crystal precipitation is a common problem during crystal growth. While the macro integrity of the crystal structure remains intact, the number of impurities entering the lattice depends on factors as such the solubility and migration speed of impurities in the melt, ionic radius of impurities, charge, degree of mismatch with component ions, and crystal growth speed. The segregation coefficient (K_α) of impurities in BSO crystals can be used as an indicator of the high (K_α>1) or low (K_α<1) affinity of the element to the BSO matrix. The K_α were calculated as follows:

$$K_\alpha = C_{Heel} / C_{Top}$$

where C_{Heel} is the concentration of elements at the heel of the crystal, and C_{Top} is the concentration of elements at the top of the crystal. Therefore, it is important to identify the K_α of various impurities, particularly those that impact the properties of a crystal. Impurities were quantified using LA-ICP-MS by ablating the crystal from the bottom to top along the axial their positions. The relationship between impurities and position in the axial direction is shown in Fig. S1. The impurity K_α in the BSO crystals were then analyzed based on the impurity concentrations at the top and bottom of the BSO crystal samples, as listed in Table 3. Because the crystals are not representative of the original crystals Owing to post-processing such as cutting and polishing, the specific value of K_α is not given.

Table 2. Comparison of LA-ICP-MS and PN-ICP-MS trace element analysis of BSO crystals

Isotope	Value (μg/g)		R^2	LOD (ng/g)
	LA-ICP-MS	PN-ICP-MS		
^{24}Mg	3.79±0.27	4.14±0.31	0.993	17
^{45}Sc	0.71±0.06	0.67±0.03	0.999	57
^{48}Ti	5.70±0.75	6.44±0.35	0.995	48
^{90}Zr	2.76±0.20	2.61±0.12	0.994	5
^{139}La	2.31±0.22	2.13±0.14	0.994	7
^{146}Nd	1.28±0.06	1.37±0.05	0.995	16
^{172}Yb	0.21±0.04	0.20±0.01	0.999	27
^{208}Pb	7.40±0.31	7.08±0.22	0.994	7

Table 3. Summary of distribution for elemental impurity concentration at the top and bottom of the crystal and their impurity segregation coefficients (K_α)

Elements	Zonal impurity concentration (μg/g)		K_α
	Tip	Heel	
^{24}Mg	2.67±0.17	4.14±0.31	-
^{45}Sc	0.84±0.05	0.67±0.03	<1
^{48}Ti	4.02±0.12	6.44±0.35	>1
^{90}Zr	0.15±0.02	2.61±0.12	>1
^{139}La	0.21±0.02	2.13±0.14	>1
^{146}Nd	0.25±0.01	1.37±0.05	>1
^{172}Yb	1.05±0.09	0.20±0.01	<1
^{208}Pb	1.51±0.06	7.08±0.22	>1

Accordingly, they can be classified into three types: The first type is distributed gradually from the bottom of the crystal to top. For example, ^{45}Sc, and ^{172}Yb, were enriched at the top of the crystal, and the K_α value wash less than 1. The second type of impurity has an opposite distribution to the first, with the amount of impurity, gradually increasing from the bottom to the top of crystal. For example, ^{48}Ti, ^{90}Zr, ^{139}La, ^{146}Nd, ^{157}Gd, and ^{208}Pb impurities exhibit K_α greater than 1. The third group of impurities lacks obvious regularity, such as ^{24}Mg. Using these K_α values, the relative ease of removing these trace impurities from the BSO lattice can be determined. This information on trace impurity elements also helps predict their effect on defect formation in BSO crystals.

Trace element quantitative imaging of microscopic defects. Impurities entering the lattice during crystal precipitation to fill gaps or as substitutions can lead to defect formation during crystal growth. As shown in Fig. 3a, feather-like defects usually appear during the growth of BSO crystals, which seriously affect the scintillation performance of the crystals and limit the growth of

Fig. 3 BSO sample and distribution images of ^{45}Sc (c) and ^{172}Yb (d) by LA-ICP-MS mapping (Fig. 3a: Physical crystals; Fig. 3b: Area of laser ablation).

Fig. 4 Pictures of the area of ablation and the distribution of elements as measured by LA-ICP-MS mapping: (a) area of laser ablation, (b) distribution of ^{48}Ti, (c) distribution of ^{90}Zr, (d) distribution of ^{139}La, (e) distribution of ^{146}Nd, (f) distribution of ^{208}Pb.

large crystals. After processing the crystal into a $1 \times 1 \times 0.1$ cm^3 sheet, the feather-like defect region was exposed, and the region contained many dendritic crystal defects with a width of approximately several tens of microns. It was hypothesized that microscopic dendritic crystal defects cause the macroscopic feathery defects and the formation of dendritic crystal defects is closely related to impurities in the crystal. However, not of these impurities are harmful impurities, and some are even beneficial.

Therefore, after clarifying the relationship between impurities and crystal defect formation, it is important to strictly limit harmful impurities and consciously mix in the beneficial impurities.

Impurities in the dendritic crystal defect region (Fig. 3b) were imaged using LA-ICP-MS to investigate, the relationship between the impurities and dendritic crystal defect formation. As shown in Fig. 3b, the imaging area contains micrographs of four dendritic defects. The LA-ICP-MS facilitates, the comparison between the elemental distribution images and the morphologies of the real samples. The quantitative elemental distribution maps of Mg, Sc, Ti, Zr, La, Nd, Yb and Pb were generated using the by LA-ICP-MS line scans of the region (Fig. 3b). The images visualize the difference in the distribution of impurity elements in the dendritic crystal defects and normal regions of the crystal. As shown in Figs. 3c and 3d, ^{45}Sc and ^{172}Yb were enriched in the dendritic crystal defects as ^{45}Sc and ^{172}Yb content were much higher than in the normal region. Furthermore, as shown in Fig. 4, ^{48}Ti, ^{90}Zr, ^{139}La, ^{146}Nd, ^{157}Gd, and ^{208}Pb were enriched in the normal region of the crystal, while their content was very low in the region of dendritic crystal defects. In addition, as far as the imaging results are concerned, there is no obvious pattern in the distribution of ^{24}Mg.

Analysis of the K_α of impurities (Table 3) reveals the relationship between an element's coefficient and its distribution patterns. Elements with a K_α greater than 1 (^{48}Ti, ^{90}Zr, ^{139}La, ^{146}Nd, and ^{208}Pb) showed reduced concentration in the defect regions compared to the normal crystal region. Comparatively, the ^{45}Sc and ^{172}Yb, which had a K_α of lower than one, showed increased concentration in the defect compared to the normal region. Finally, there was no observable segregation effect observed for ^{24}Mg. As such, it was concluded that impurities with a K_α greater than one, such as ^{48}Ti, ^{90}Zr, ^{139}La, ^{146}Nd, and ^{208}Pb, inhibit the formation of dendritic crystal defects in BSO crystals, and the content of these impurity elements in the crystal raw material can be appropriately relaxed. Conversely, ^{45}Sc and ^{172}Yb, which have K_α less than 1, promote the formation of dendritic crystal defects in BSO crystals, and the content of these impurity elements in the crystal raw material should be strictly controlled. The effect of impurities such as ^{24}Mg on the formation of dendritic crystal defects in BSO crystals is unclear.

CONCLUSION

A novel method based on LA-ICP-MS, combined with the preparation and use of matrix-matched calibration standards, was developed for the quantitative imaging analysis of trace impurity elements in BSO crystals. Through measurement and imaging of the distribution patterns of trace impurity elements in the different morphological areas of BSO crystal, a relationship between the K_α of impurity elements and the influence of impurity elements on the formation of dendritic crystal defects was established. The elements ^{48}Ti, ^{90}Zr, ^{139}La, ^{146}Nd, and ^{208}Pb, with K_α great than 1, inhibited the formation of dendritic crystal defects in the BSO crystals. Conversely, ^{45}Sc, and ^{172}Yb, which have K_α less than 1, favored the formation of dendritic crystal defects in the BSO crystals. This study shows the possibility of growing large, and high-quality crystals at a reduced cost by reducing the amount of harmful impurities and incorporating beneficial impurities in the raw material. Furthermore, this study displays the applicability of LA-ICP-MS for the analysis of crystal components and properties. The results of this preliminary study are promising for further investigations on the mechanistic role of trace impurity elements in the formation of crystal defects in BSO crystals.

ASSOCIATED CONTENT

The supporting information (Fig. S1) is available at www.at-spectrose.com/as/home.

AUTHOR INFORMATION

Zheng Wang received his PhD in 2006 from the Shanghai Institute of Ceramics, Chinese Academy of Sciences (CAS). He is a research professor and PhD supervisor at the Shanghai Institute of Ceramics, CAS. His major research interests are environmental analytical chemistry, spectroscopy instrument development, preparation and characterization of new inorganic materials, 3D printing materials and precision manufacturing, etc. He has been working as member of editorial board for *Atomic Spectroscopy*, *Chinese Chemical Letters,* and *Spectroscopy and Spectral Analysis*. Zheng Wang is author or co-author of over 100 articles published in peer-reviewed scientific journals. In 2010 and 2018, he received two science and technology awards from the China Association for Analysis and Testing.

Corresponding Author

* J.Y. Xu

Email address: 2631274244@qq.com

* Z. Wang

Email address: wangzheng@mail.sic.ac.cn

Notes

The authors declare no competing financial interest.

ACKNOWLEDGMENTS

This work was supported by the National Natural Science

Foundation of China (52203302), and Science and Technology Innovation Project of Shanghai Institute of Ceramics, the Shanghai Technical Platform for Testing and Characterization on Inorganic Materials (19DZ2290700).

REFERENCES

1. M. J. Weber, *J. Lumin.*, 2002, **100**, 35-45. https://doi.org/10.1016/S0022-2313(02)00423-4
2. B. C. Grabmaier, *J. Lumin.*, 1994, **60-61**, 967-970. https://doi.org/10.1016/0022-2313(94)90322-0
3. N. Martin, *Meas. Scl. Technol.*, 2006, **17**, R37. https://doi.org/10.1134/S0020441216030192
4. N. Senguttuvan, N. Kidokoro, K. Ootsuka, M. Ishii, and S. Kurimura, *J. Cryst. Growth.*, 2001, **229**, 188-192. https://doi.org/10.1016/S0022-0248(01)01118-6
5. Y. Fei, R. Sun, M. Ishii, and S. Fan, *Prog. Cryst. Growth. Charact. Mater*., 2000, **40**, 183-188. https://doi.org/10.1016/S0960-8974(00)00003-6
6. N. Akchurin, *Nucl. Instrum. Meth*., 2011, **640**, 91-98. https://doi.org/10.1016/j.nima.2011.03.013
7. Y. T. Fei, S. J. Fan, R. Y. Sun, and J. Y. Xu, *Prog. Cryst. Growth. Charact. Mater*., 2000, **40**, 189-194. https://doi.org/10.1016/S0960-8974(00)00004-8
8. F. Yang, H. Yuan, L. Zhang, and R. Y. Zhu, *J. Phys. Confer. Seri.*, 2015, **587**, 12064-12064. https://doi.org/10.1088/1742-6596/587/1/012064
9. A.S. Kozyrev, G. I. Mitrofanov, J. Benkhoff, A. Owens, F. Quarati, M. L. Litvak, M. I. Malakhov, G.N. Timoshenko, and V. N. Shvetsov, *Instrum. Exp. Tech*., 2016, **59**, 569-577. https://doi.org/10.1134/S0020441216030192
10. C. Pedrini, *Phys. Solid. State*., 2005, **47**, 1406-1411. https://doi.org/10.1134/1.2014478
11. Y. Wang, H. Li, M. Raikes, and B. Linehan, *Cryst. Growth. Des*., 2021, **21**, 4100-4110. https://doi.org/10.1021/acs.cgd.1c00399
12. H. Miura and K. Tsukamoto, *Cryst. Growth. Des*., 2013, **13**, 3588-3595. https://doi.org/10.1021/jp309550y
13. S. Seif, J. M. Chang, K. Bhat, B. Penn, and R. B. Lal, *Cryst. Growth. Des*., 2001, 1, 359-362. https://doi.org/10.1021/cg010002a
14. K. Yoshizawa, T. Okuzono, T. Koga, T. Taniji, and J. Yamanaka, *Langmuir*., 2011, **27**, 13420-13427. https://doi.org/10.1021/la202899v
15. S. Hu, J. Nozawa, H. Koizumi, K. Fujiwara, and S. Uda, *Cryst. Growth. Des*., 2015, **15**, 5685-5692. https://doi.org/10.1021/acs.cgd.5b00646
16. Q. Li, Z. Q. Cai, Y. Fang, and Z. Wang, *At. Spectrosc*., 2021, **42**, 238-246. https://doi.org/10.46770/AS.2021.019
17. R. Clough, C. F. Harrington, S. J. Hill, Y. Madrid, and J. F. Tyson, *J. Anal. At. Spectrom*., 2020, **35**, 1236-1278. https://doi.org/10.1039/c8ja90025f
18. U. Makanda, A. Voinot, R. Kandel, Y. Wu, M. Leybourne, and P. Wang, *J. Anal. At. Spectrom*., 2020, **35**, 2672-2678. https://doi.org/10.1039/D1JA90049H
19. J. Hirata, D. Itabashi, and M. Aimoto, *Anal. Sci*., 2021, **37**, 1757-1763. https://doi.org/10.2116/analsci.21P143
20. A. Scordo , L. Breschi, C. Curceanu, M. Miliucci, F. Sirghi, and J. Zmeskal, *J. Anal. At. Spectrom*., 2020, **35**, 155-168. https://doi.org/10.1039/D2JA90049A
21. M. G. Abramson, I. A. Saprykina, S. E. Kichanov, D. P. Kozlenko, and K. M. Nazarov, *J. Surf. Invest-X-RAY*., 2018, **12**, 114-117. https://doi.org/10.1134/S1027451018010202
22. A. Scordo , L. Breschi, C. Curceanu, M. Miliucci, F. Sirghi, and J. Zmeskal, *J. Anal. At. Spectrom*., 2020, **35**, 155-168. https://doi.org/10.1039/D2JA90049A
23. S. Mushtaq, E. B. M. Steers, J. A. Whitby, P. Horvath, J. Michler, and J. C. Pickering, *J. Anal. At. Spectrom*., 2015, **30**, 1774-1781. https://doi.org/10.1039/C5JA00112A
24. W. Yang, S. Zhuo, Z. Zhu, R. Qian, Q. Chen, and J. Dong, *J. Anal. At. Spectrom*., 2021, **36**, 932-937. https://doi.org/10.1039/D0JA00481B
25. J. M. Carbonne, A. Kiss, A. S. Bouvier, A. Meibom, L. Baumgartner, T. Bovay, F. Plane, S. Escrig, and D. Rubatto, *Chimia*., 2022, **76**, 26-33. https://doi.org/10.2533/chimia.2022.26
26. L. White, P. M. Vasconcelos, J. N. Vila, T. Ubide, and T. R. Ireland, *Chem. Geol*., 2021, **583**, 120461. https://doi.org/10.1016/j.chemgeo.2021.120461
27. X. Llovet, A. Moy, P. T. Pinard, and J. H. Fournelle, *Prog. Mater. Sci*., 2021, **116**, 100-673. https://doi.org/10.1016/j.pmatsci.2020.100673
28. S. Wu, Y. Wang and C. Xu, *Rock. Mine. Anal*., 2015, **34**, 503-511. https://doi.org/10.15898/j.cnki.11-2131/td.2015.05.002
29. H. J. Pan, L. X. Feng, Y. L. Lu, Y. C. Han, J. P. Xiong, and H. M. Li, *Trac-Trend Anal. Chem.*, 2022, **156**, 116-710. https://doi.org/10.1016/j.trac.2022.116710
30. N. Miliszkiewicz, S. Walas, and A. Tobiasz, *J. Anal. At. Spectrom*., 2015, **30**, 327-338. https://doi.org/10.1039/C4JA00325J
31. Y. Liu, W. Wang, W. Ling, T. Zhang, X. Wang, Q. Liu, and G. Jiang, *J. Instrum. Anal*., 2021, **40**, 767-776. https://doi.org/10.3969/j.issn.1004-4957.2021.05.021
32. Q. Li, Y. Fang, J. H. Liu, C. G. Zhang, and Z. Wang, *At. Spectrosc*., 2021, **42**, 154-159. https://doi.org/ 10.46770/AS.2021.101
33. W. X. Cui, Z. Q. Cai, Q. Li, H. Y. Qu, J. Q. Zheng, D. G. Yu, J. F. Chen, and Z. Wang, *Talanta*., 2023, **255**, 124–248. https://doi.org/10.1016/j.talanta.2022.124248
34. Y. Zhu, C. Li, M. Chen, G. Zhang, C. Mao, H. Kou, and Z. Wang, *At. Spectrosc*., 2019, **40**, 49-54. https://doi.org/10.46770/AS.2019.02.003